High precision and continuous optical transport using a standing wave optical line trap

Vassili Demergis and Ernst-Ludwig Florin*

The University of Texas at Austin, Department of Physics, Center for Nonlinear Dynamics, 1 University Station C1600, Austin, Texas 78712, USA

**florin@chaos.utexas.edu*

http://chaos.utexas.edu/

Abstract: We introduce the Standing Wave Optical Line Trap (SWOLT) as a novel tool for precise optical manipulation and long-range transport of nano-scale objects at low laser power. We show that positioning and transport along the trap can be achieved by controlling the lateral component of the scattering force while the confinement of the particles by the gradient force remains unaffected. Multiple gold nanoparticles with a diameter of 100nm were trapped at a power density 3 times smaller than previously reported while their transverse fluctuations remained sufficiently small ($\pm 36nm$) to maintain the order of the particles. The SWOLT opens new doors for sorting, mixing, and assembly of synthetic and biological nanoparticles.

OCIS codes: (000.2170) Equipment and techniques; (120.4640) Optical instruments; (140.7010) Laser trapping; (170.4520) Optical confinement and manipulation; (350.4855) Optical tweezers or optical manipulation.

References and links

1. A. Ashkin, J. M. Dziedzic, J. E. Bjorkholm, and S. Chu, "Observation of a single-beam gradient force optical trap for dielectric particles," Opt. Lett. **11,** 288–290 (1986).
2. A. Ashkin and J. M. Dziedzic, "Optical trapping and manipulation of viruses and bacteria," Science **235,** 1517–1520 (1987).
3. K. Svoboda and S. M. Block, "Biological applications of optical forces," Annu. Rev. Bioph. Biom. **23,** 247–285 (1994).
4. D. G. Grier, "A revolution in optical manipulation," Nature **424,** 810–816 (2003).
5. K. C. Neuman and S. M. Block, "Optical trapping," Rev. Sci. Instrum. **75,** 2787–2809 (2004).
6. M. Dienerowitz, M. Mazilu, and K. Dholakia, "Optical manipulation of nanoparticles: a review," J. Nanophotonics **2,** 021875 (2008).
7. A. Jonáš and P. Zemánek, "Light at work: the use of optical forces for particle manipulation, sorting, and analysis," Electrophoresis **29,** 4813–4851 (2008).
8. P. T. Korda, M. B. Taylor, and D. G. Grier, "Kinetically locked-in colloidal transport in an array of optical tweezers," Phys. Rev. Lett. **89,** 1–4 (2002).
9. M. P. MacDonald, L. Paterson, K. Volke-Sepulveda, J. Arlt, W. Sibbett, and K. Dholakia, "Creation and manipulation of three-dimensional optically trapped structures," Science **296,** 1101–1103 (2002).
10. M. P. MacDonald, G. C. Spalding, and K. Dholakia, "Microfluidic sorting in an optical lattice," Nature **426,** 421–424 (2003).
11. J. Glückstad, "Sorting particles with light," Nature Materials **3,** 9–10 (2004).
12. M. Pelton, K. Ladavac, and D. G. Grier, "Transport and fractionation in periodic potential-energy landscapes," Phys. Rev. E **70,** 1–10 (2004).

#152071 - $15.00 USD Received 1 Aug 2011; revised 8 Sep 2011; accepted 8 Sep 2011; published 5 Oct 2011

13. Y. Roichman, V. Wong, and D. G. Grier, "Colloidal transport through optical tweezer arrays," Phys. Rev. E **75,** 1–4 (2007).
14. K. Sasaki, M. Koshioka, H. Misawa, N. Kitamura, and H. Mashuhara, "Pattern formation and flow control of fine particles by laser-scanning micromanipulation," Opt. Lett. **16,** 1463–1465 (1991).
15. L. P. Faucheux, L. S. Bourdieu, P. D. Kaplan, and A. J. Libchaber, "Optical thermal ratchet," Phys. Rev. Lett. **74,** 1504–1507 (1995).
16. L. P. Faucheux, G. Stolovitzky, and A. Libchaber, "Periodic forcing of a Brownian particle," Phys. Rev. E **51,** 5239–5250 (1995).
17. C. Mio, T. Gong, A. Terray, and D. W. M. Marr, "Design of a scanning laser optical trap for multiparticle manipulation," Rev. Sci. Instrum. **71,** 2196–2200 (2000).
18. R. Dasgupta, S. K. Mohanty, and P. K. Gupta, "Controlled rotation of biological microscopic objects using optical line tweezers," Biotechnol. Lett. **25,** 1625–1628 (2003).
19. B. Liesfeld, R. Nambiar, and J. C. Meiners, "Particle transport in asymmetric scanning-line optical tweezers," Phys. Rev. E **68,** 1–6 (2003).
20. R. W. Applegate Jr., J. Squier, T. Vestad, J. Oakey, and D. W. M. Marr, "Optical trapping, manipulation, and sorting of cells and colloids in microfluidic systems with diode laser bars," Opt. Express **12,** 4390–4398 (2004).
21. R. Nambiar, A. Gajraj, and J.-C. Meiners, "All-optical constant-force laser tweezers," Biophys. J **87,** 1972–80 (2004).
22. S. K. Mohanty and P. K. Gupta, "Transport of microscopic objects using asymmetric transverse optical gradient force," Appl. Phys. B **81,** 159–162 (2005).
23. F. C. Cheong, C. H. Sow, A. T. S. Wee, P. Shao, A. A. Bettiol, J. A. van Kan, and F. Watt, "Optical travelator: transport and dynamic sorting of colloidal microspheres with an asymmetrical line optical tweezers." Appl. Phys. B **83,** 121–125 (2006).
24. M. Khan, A. K. Sood, S. K. Mohanty, P. K. Gupta, G. V. Arabale, K. Vijaymohanan, and C. N. R. Raol, "Optical trapping and transportation of carbon nanotubes made easy by decorating with palladium," Opt. Express **14,** 424–429 (2006).
25. Y. Roichman and D. G. Grier, "Projecting extended optical traps with shape-phase holography," Opt. Lett. **31,** 1675–1677 (2006).
26. A. V. Arzola, K. Volke-Sepúlveda, and J. L. Mateos, "Experimental control of transport and current reversals in a deterministic optical rocking ratchet," Phys. Rev. Lett. **106,** 168104 (2011).
27. D. McGloin, V. Garcés-Chávez, and K. Dholakia, "Interfering Bessel beams for optical micromanipulation," Opt. Lett. **28,** 657–659 (2003).
28. T. Čižmár, V. Garcéz-Chávez, K. Dholakia, and P. Zemánek, "Optical conveyor belt based on Bessel beams," Proc. SPIE **5930,** 231–237 (2005).
29. T. Čižmár, V. Garcés-Chávez, K. Dholakia, and P. Zemánek, "Optical conveyor belt for delivery of submicron objects," Appl. Phys. Lett. **86,** 174101 (2005).
30. T. Čižmár, V. Kollárová, M. Šiler, P. Jákl, Z. Bouchal, V. Garcés-Chávez, K. Dholakia, and P. Zemánek, "Non-diffracting beam synthesis used for optical trapping and delivery of sub-micron objects," Proc. SPIE **6195,** 619507 (2006).
31. M. Šiler, T. Čižmár, M. Šerý, and P. Zemánek, "Optical forces generated by evanescent standing waves and their usage for sub-micron particle delivery," Appl. Phys. B **84,** 157–165 (2006).
32. T. Čižmár, M. Šiler, M. Šerý, P. Zemánek, V. Garcés-Chávez, and K. Dholakia, "Optical sorting and detection of submicrometer objects in a motional standing wave," Phys. Rev. B **74,** 1–6 (2006).
33. T. Čižmár, M. Šiler, and P. Zemánek, "An optical nanotrap array movable over a milimetre range," Appl. Phys. B **84,** 197–203 (2006).
34. M. Šiler, T. Čižmár, A. Jonáš, and P. Zemánek, "Delivery of multiparticle chains by an optical conveyor belt," Proc. SPIE **7138,** 713822 (2008).
35. M. Šiler, T. Čižmár, A. Jonáš, and P. Zemánek, "Surface delivery of a single nanoparticle under moving evanescent standing-wave illumination," New J. Phys. **10,** 113010 (2008).
36. T. Čižmár, O. Brzobohatý, K. Dholakia, and P. Zemánek, "The holographic optical micro-manipulation system based on counter-propagating beams," Laser Phys. Lett. **8,** 50–56 (2011).
37. P. Zemánek, A. Jonáš, L. Šrámek, and M. Liška, "Optical trapping of Rayleigh particles using a Gaussian standing wave," Opt. Commun. **151,** 273–285 (1998).
38. P. Zemánek, A. Jonáš, L. Šrámek, and M. Liška, "Optical trapping of nanoparticles and microparticles by a Gaussian standing wave," Opt. Lett. **24,** 1448–50 (1999).
39. P. Jákl, A. Jonáš, E.-L. Florin, and P. Zemánek, "Comparison of the single beam and the standing wave trap stiffnesses," Proc. SPIE **4356,** 347–352 (2001).
40. A. Jonáš, P. Zemánek, and E.-L. Florin, "Single-beam trapping in front of reflective surfaces," Opt. Lett. **26,** 1466–8 (2001).
41. P. Zemánek, A. Jonáš, and M. Liška, "Simplified description of optical forces acting on a nanoparticle in the Gaussian standing wave," J. Opt. Soc. Am. A **19,** 1025–1034 (2002).
42. P. Zemánek, A. Jonáš, P. Jákl, J. Ježek, M. Šerý, and M. Liška, "Theoretical comparison of optical traps created

#152071 - $15.00 USD Received 1 Aug 2011; revised 8 Sep 2011; accepted 8 Sep 2011; published 5 Oct 2011

by standing wave and single beam," Opt. Commun. **220,** 401–412 (2003).
43. H. Fujiwara, H. Takasaki, J. Hotta, and K. Sasaki, "Observation of the discrete transition of optically trapped particle position in the vicinity of an interface," Appl. Phys. Lett. **84,** 13 (2004).
44. S. Zwick, T. Haist, Y. Miyamoto, L. He, M. Warber, A. Hermerschmidt, and W. Osten, "Holographic twin traps," J. Opt. A: Pure Appl. Opt. **11,** 034011 (2009).
45. M. Pitzek, R. Steiger, G. Thalhammer, S. Bernet, and M. Ritsch-Marte, "Optical mirror trap with a large field of view," Opt. Express **17,** 19414–19423 (2009).
46. R. Bowman, A. Jesacher, G. Thalhammer, G. Gibson, M. Ritsch-Marte, and M. Padgett, "Position clamping in a holographic counterpropagating optical trap," Opt. Express **19,** 9908–9914 (2011).
47. W. M. Lee, P. J. Reece, R. F. Marchington, N. K. Metzger, and K. Dholakia, "Construction and calibration of an optical trap on a fluorescence microscope." Nat. Protoc. **2** 3226–3238 (2007).
48. P. M. Hansen, V. K. Bhatia, N. Harrit, and L. Oddershede, "Expanding the optical trapping range of gold nanoparticles," Nano. Lett. **5,** 1937–1942 (2005).
49. F. Hajizadeh and S. N. S. Reihani, "Optimized optical trapping of gold nanoparticles," Opt. Express **18,** 551–559 (2010).
50. S.-U. Hwang and Y.-G. Lee, "Simulation of an oil immersion objective lens: a simplified ray-optics model considering Abbe's sine condition," Opt. Express **16,** 21170–83 (2008).
51. J. Happel and H. Brenner, *Low Reynolds Number Hydrodynamics* (Prentice-Hall Inc., 1965).
52. M. M. Burns, J.-M. Fournier, and J. A. Golovchenko, "Optical binding," Phys. Rev. Lett. **63,** 1233–1236 (1989).
53. S. K. Mohanty, J. T. Andrews, and P. K. Gupta, "Optical binding between dielectric particles," Opt. Express **12,** 2749–2756 (2004).
54. K. Dholakia and P. Zemánek, "Colloquium: Gripped by light: Optical binding," Rev. Mod. Phys. **82,** 1767–1791 (2010).
55. T. Čižmár, L. C. Dávila Romero, K. Dholakia, and D. L. Andrews, "Multiple optical trapping and binding: new routes to self-assembly," J. Phys. B: At. Mol. Opt. Phys. **43,** 102001 (2010).
56. O. Brzobohatý, T. Čižmár, V. Karásek, M. Šiler, K. Dholakia, and P. Zemánek, "Experimental and theoretical determination of optical binding forces," Opt. Express **18,** 25389–25402 (2010).

1. Introduction

With the introduction of the optical tweezers by Ashkin in 1986 [1, 2], fields such as biophysics, colloidal physics and nanotechnology have widely adopted it as a tool for manipulating and applying external forces on micro-scale objects without being invasive to the system [3–7]. While standard optical tweezers are commonly used to manipulate single objects, the development of new methods for multi-particle manipulation has recently become of great interest. For example, optical methods for sorting and mixing of particles as part of lab-on-chip devices have been the focus of many studies, also known as optical fractionation [8–13]. There has also been much effort in optical methods for continuous transport and delivery of many particles along defined pathways in extended optical traps [14–26]. However, both the optical fractionation and extended trap techniques have only been shown to be effective for manipulating individual particles larger than about $1\mu m$ in diameter.

There are some techniques which have demonstrated simultaneous manipulation of smaller particles using counter-propagating Bessel beams or evanescent interfering fields [27–36]. Particles even as small as $200nm$ in diameter were shown to be manipulated [30, 31, 33, 35]. However, manipulating such small particles seemed to require laser power of more than $1W$. Such high powers would likely damage biological samples, and laser heating of the sample has been reported as a problem in at least one instance utilizing Bessel beams [30]. And while the laser power used in the evanescent interfering field technique may be distributed over a larger area, the particles are pulled toward the surface by the gradient force and are not trapped free floating in solution, which could make controlled assembly of particles difficult.

Our goal is to develop a technique that can manipulate nanoparticles free in solution using low laser power and allows for continuous optical transport. Such a technique would be highly beneficial for sorting, mixing and assembly of not only synthetic particles such as individual carbon nanotubes, but also for biological particles such as small vesicles. With this goal in mind, we base our technique on the standing wave optical trap (SWOT), which has been shown

#152071 - $15.00 USD Received 1 Aug 2011; revised 8 Sep 2011; accepted 8 Sep 2011; published 5 Oct 2011

to produce stronger intensity gradients and deeper potential wells compared to a single beam trap (SBT) of the same power and is able to trap nanoparticles free in solution [37–43]. In a SBT, a laser beam is typically focused by a high numerical aperture lens in order for the axial gradient force to overcome the axial scattering force. This requirement is eliminated in a SWOT due to the compensation of the axial scattering force by the reflected beam [37–46] and because the axial gradient force is still generated by the standing wave pattern even if collimated beams are used. This advantage allows us to generate a highly stable standing wave optical line trap (SWOLT), even though we have only focused the trapping beam in one dimension. We use the SWOLT to confine nanoparticles to a precise pathway where the transverse thermal position fluctuations of the particles are still smaller than their diameter. This is important, for example, for the precise ordering and assembly of nano-objects.

While the precise confinement of nano-particles is a necessary step in an assembly process, it would be desirable if the particles could be manipulated independent of this confinement. Here we show that the *lateral* component of the scattering force can be used for unidirectional or bidirectional continuous transport out of the trap or for forcing the aggregation of particles. The lateral component of the scattering force can be controlled by the lateral and axial position of the cylinder lens that is used to generate the SWOLT, while the confinement by the gradient force remains unaffected. The action of the lateral scattering force can be understood by a simple ray optics model that takes into account the change of incident angle of the trapping beam as a function of cylinder lens position.

2. Experimental design

The design of the SWOLT is similar to that of standard single beam traps but with a few additions. Fig. 1 shows a schematic diagram of our SWOLT. The system is designed around an inverted microscope (Axiovert 100, Carl Zeiss, Germany). Objects are imaged using the microscope's built-in differential interference contrast (DIC) components which include the condenser lens, Wollaston prisms, polarizer, analyzer and a halogen lamp as the light source. A CCD camera (Rolera-XR Fast Cooled, Q-Imaging, Surrey, BC, Canada) is used to capture real time videos of the particles. A 1064nm wavelength single longitudinal mode laser (CL1064-1W0-S, CrystaLaser, Reno, NV, USA) is coupled into a single mode polarization preserving fiber optic cable (PMC-980/1064-6 4-NA012-3-APC-500-P, Schäfter and Kirchoff GmbH, Germany). The coupling optics of the fiber expand the beam to about 5mm in diameter in order to overfill the back aperture of the objective lens. The objective lens (Plan-Neofluar 100x/1.3 Oil Pol, Carl Zeiss, Germany) is used both for imaging and for focusing the laser onto the surface of a dichroic coverslip (1064nm reflectivity $> 99\%$). The incident and reflected laser beams interfere and generate a standing wave trap within the sample chamber (see Fig. 1 inset). The sample chamber volume is typically filled with deionized water along with the sample to be studied. A $\lambda/2$ plate is used to change the polarization angle of the incident laser beam such that it is not split in two by the Wollaston prism. Finally, a cylinder lens (LJ1653RM-C, $f = 200mm$, Thorlabs, Newton, NJ) is inserted in the beam path in order to transform the SWOT into a SWOLT. This is done by focusing the laser beam onto a line localized on the back focal plane of the objective and centered on the optical axis. We will call this the "default" alignment. The first trapping volume near the dichroic coverslip is nearly diffraction limited transverse to the long axis (y-axis) of the line trap. The width of the elongated Gaussian intensity profile along the line trap (x-axis) is determined by the diameter of the incident laser beam, the focal length of the cylinder lens, and the back focal length of the objective lens. The focusing axis of the cylinder lens (x_{CL}-axis) corresponds to the elongated axis of the trapping beam (x-axis), thus the SWOLT can also be rotated through rotation of the cylinder lens. We will show that particles can be manipulated by translating the cylinder lens laterally or axially from the default

#152071 - $15.00 USD Received 1 Aug 2011; revised 8 Sep 2011; accepted 8 Sep 2011; published 5 Oct 2011

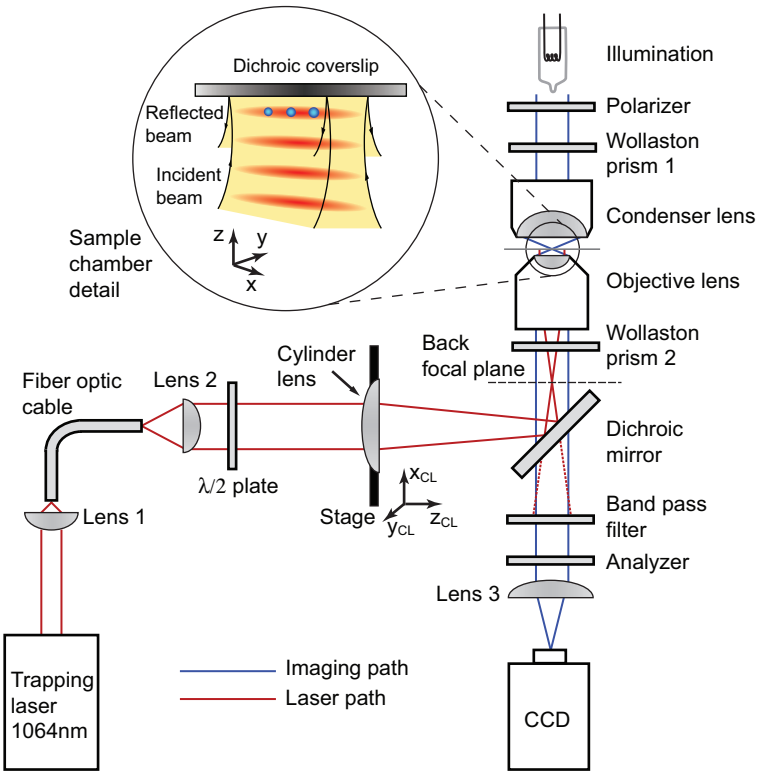

Fig. 1. Schematic of a standing wave optical line trap. The design is based on a standard single beam trap design [5, 47], but with two additions. A dichroic coverslip is used as part of the sample chamber to generate a standing wave optical trap. The cylinder lens is used to stretch the trapping volume into a line, and translation of the cylinder lens generates lateral components of scattering force which drive transport along the line.

position. Thus, the cylinder lens is mounted on an XY stage for precise translation perpendicular to the beam path, and the XY stage is attached to a rail system that permits long-range translation of the cylinder lens along the optical axis. This allows the cylinder lens focal line to be positioned relative to the back focal plane of the objective lens in order to generate either collimated, converging, or diverging trapping beams within the sample.

3. Results and discussion

The ability of the SWOLT to stably trap and align nanoparticles at low laser power is demonstrated in Fig. 2. The compensation of the scattering force increases the stability of the SWOLT

Fig. 2. Trapping and alignment of nanoparticles in the SWOLT. Gold particles 100nm in diameter were stably trapped and aligned in the SWOLT with 70mW of laser power in the focal plane. Particles are imaged using dark-field microscopy. The particle second from the left is trapped in the second antinode of the standing wave and thus is out of focus.

#152071 - $15.00 USD Received 1 Aug 2011; revised 8 Sep 2011; accepted 8 Sep 2011; published 5 Oct 2011

when compared to a single beam trap (SBT). Particularly for metallic particles in a SBT, the strong scattering forces push them along the optical axis to positions away from intensity maximum where they become less stable. Thus higher laser powers are generally required for stable trapping compared to a SWOT. For example, 97 nm diameter gold particles were trapped with 30mW of laser power in an optimized SBT [48, 49]. Here we use 70mW, but when comparing the theoretical power density of the diffraction limited Gaussian focal spot of the SBT ($\sigma_x = \sigma_y \approx 0.5\mu m$) with the extended SWOLT ($\sigma_x \approx 15\mu m$, measured from direct images of the SWOLT intensity profile, and $\sigma_y \approx 0.5\mu m$), and even accounting for a factor of 4 increase in power density due to the standing wave, the required power density of the SWOLT is still at least 3 times lower at the intensity maximum. Particles were also stably trapped far away from the intensity maximum of the SWOLT (along the *x*-direction) where the power density can be nearly an order of magnitude lower compared to the center of the SBT.

Despite the low power density, the gold nanoparticles are well aligned within the SWOLT. Using video analysis to track the particle positions, the measured standard deviation of the transverse (*y*-axis) thermal fluctuations along the length of the trap explored by the particles is only $36 \pm 4nm$ (determined by a Gaussian fit to the position data) which is smaller than their radius. Thus the probability that they reorder themselves along the SWOLT is very low which is desirable for the assembly of nanoparticles in a precise order.

While it is possible to trap, align, and manipulate such small particles in the SWOLT, their diameter is below the diffraction limit. This makes the quantification of the trap properties difficult. Although we can distinguish individual 100nm gold particles from aggregates based on the scattering intensity (for example doublets appear roughly twice as bright as an individual), the center of an individual particle cannot be tracked if particles aggregate. Therefore, we use 500nm diameter polystyrene particles, easily resolved in conventional DIC microscopy, for all following experiments which will characterize the SWOLT.

To determine the trap stability we observed a 500nm diameter polystyrene particle diffusing in the SWOLT for 2 hours (see Fig. 3(a)) and calculated the position histogram. The longitudinal (*x*-axis) as well as the transverse (*y*-axis) probability distributions follow a Gaussian profile that corresponds to a harmonic potential. The width of the probability distribution along the *x*-axis (at $y = 0$) is $385 \pm 4nm$ and along the *y*-axis (at $x = 0$) is $36.9 \pm 0.4nm$. The corresponding spring constants are $k_x = 0.025 \pm 0.002 pN/\mu m$ and $k_y = 2.6 \pm 0.2 pN/\mu m$. The errors in these values are determined from least-squares fitting of the data. The small fluctuations along the *y*-axis underline the strong transverse confinement of the particle by SWOLT while the confinement along the trap is weak, allowing the particle to explore more than two micrometers by thermal excitation. The aspect ratios are approximately 10:1 for the position fluctuations and 1:100 for the force constants. As expected, the transverse force constant k_y is nearly invariant over the explored length of the trap (see Fig. 3(b)) which indicates a tube-like confinement of the particle. The uniform transverse confinement also suggests that the SWOLT extends much further out, but these parts of the SWOLT are not accessible by thermal fluctuations under the given experimental conditions. To also explore these parts of the SWOLT, we use two additional methods: change of the average particle position by the lateral component of the scattering force and the measurement of the flow velocity of the particle after it is captured by the SWOLT.

In the experiment described above, the SWOLT was aligned so that the scattering force from the incoming and reflected beam compensated each other completely, i.e. when the trapping beam along the *x*-direction is normal to the dichroic coverslip. However, the situation where the scattering force is completely compensated is only a special case of the SWOLT. The collimated beam parallel to the optical axis (*z*-axis) is generated in the sample chamber by focusing the trapping laser beam on the center of the back focal plane of the objective lens. By translating the cylinder lens perpendicular to the optical path, a lateral component of the scattering force

#152071 - $15.00 USD Received 1 Aug 2011; revised 8 Sep 2011; accepted 8 Sep 2011; published 5 Oct 2011

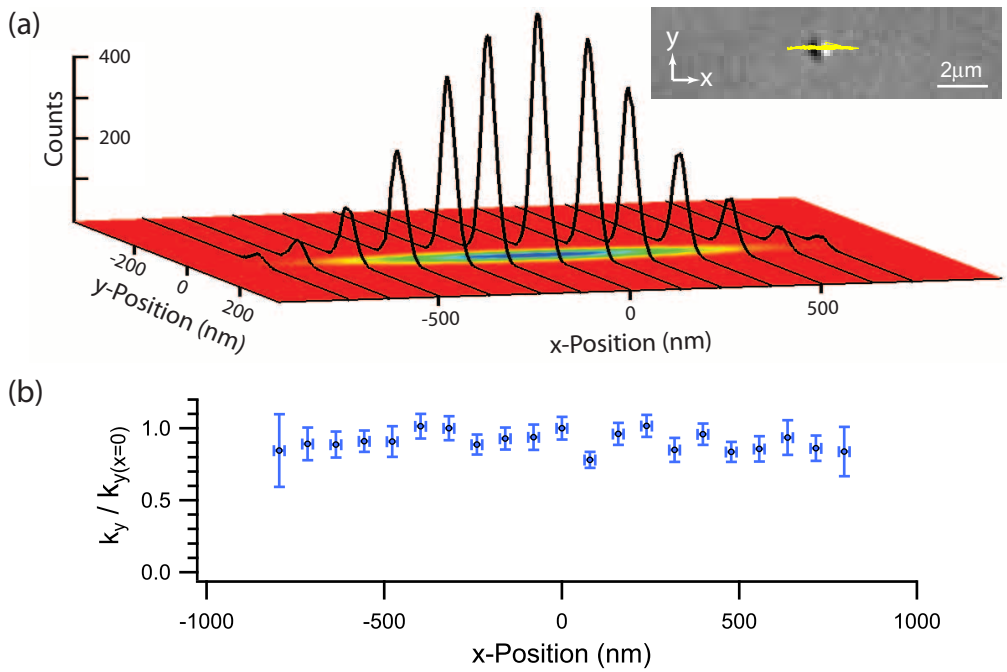

Fig. 3. Characterization of the SWOLT's trapping potential. a) Position histogram of a 500nm diameter polystyrene bead diffusing in the SWOLT for 117 minutes (1.4×10^5 data points). The base image shows the full 2D histogram data. The black curves are individual line profiles of histogram data for a given x-position averaged over $\pm65nm$. The inset shows a sample DIC image used to track the bead. The yellow line indicates the path of the center of the particle over 30sec. b) The transverse spring constant k_y of the trap at different positions along the trap length. Values are normalized to the value at $x=0$, $k_y(0)=2.6\pm0.2pN/\mu m$. The trapping power in the focal plane was about 70mW.

($\vec{F}^s_{net}$) will be generated (see Fig. 4(a)). The dashed lines show representative light rays for the case of zero net scattering force. The solid lines show the path of those rays after the cylinder lens has been shifted by δx_{CL}. The cylinder lens focal line still lies within the back focal plane of the objective lens, thus the beam still emerges as collimated, but the incident angle (θ_m) of that collimated beam changes. Since the beam no longer propagates normal to the reflective surface of the dichroic coverslip, there is a lateral component of the scattering force ($\vec{F}^s_{net}$) while the axial components of the incoming and reflected beam still cancel each other out. The lateral components of the two beams add, amplifying its strength. The lateral scattering force can be used to push particles to different regions along the length of the SWOLT. To illustrate the action of the lateral scattering force, the cylinder lens was shifted in steps of $50\mu m$, and a 2D position histogram was obtained for each position of the diffusing particle. Figure 4(b) shows the average position of the particle for different positions of the cylinder lens. Note that the particle can be pushed over a range of $30\mu m$ to $40\mu m$ by a modest shift of the cylinder lens (range of incident angles about $\pm13^\circ$) due to the strength of the lateral scattering force.

To exclude that the longitudinal shift of the particles position is caused by a longitudinal displacement of the SWOLT while changing the position of the cylinder lens, we imaged the position of the trap and analyzed its strength. Although it is expected that the shift in the average position of the trapped particle is due to the lateral scattering force, any changes in the gradient force also need to be considered since the resting position of the particle is the point where

#152071 - $15.00 USD Received 1 Aug 2011; revised 8 Sep 2011; accepted 8 Sep 2011; published 5 Oct 2011

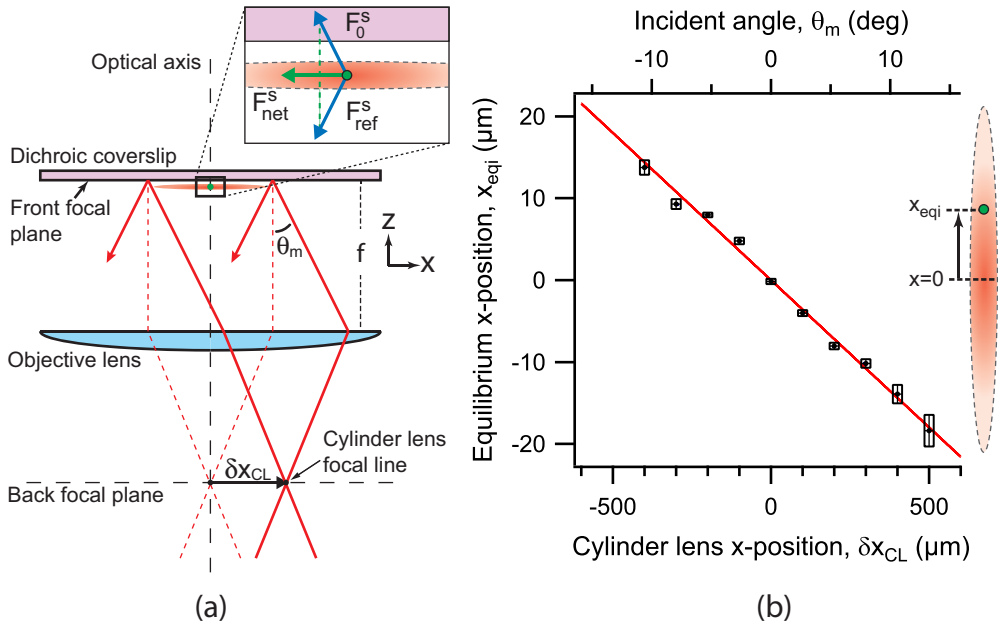

Fig. 4. Manipulation of the average particle position in the SWOLT by varying the lateral component of the scattering force. a) Ray optics diagram illustrating how the lateral component of the scattering force ($\vec{F}_{net}^s$) is generated by shifting the cylinder lens along the x_{CL}-direction. b) The average position of a trapped 500nm diameter polystyrene particle in the SWOLT is shown for different positions of the cylinder lens. The value $x_{eqi} = 0$ corresponds to a selected pixel on the CCD camera near the x-position of the intensity maximum when $\delta x_{CL} = 0$. The vertical error bars represent the standard deviation of the position. The solid red line was fit to the data using the model for the SWOLT described in the text (Eq. (9)). The incident angle (θ_m) was calculated from cylinder lens position (δx_{CL}) using Eq. (6). The inset illustrates an example of the particle position within the trapping volume's intensity profile. Parameters used: The diameter of the back aperture of the objective lens ($D = 4277\mu m$) as well as the numerical aperture ($NA = 1.3$) were given by the manufacturer; the refractive index of the medium, water, is known ($n_m = 1.33$); the longitudinal spring constant ($k_x = 25 fN/\mu m$) was measured as described in the text; and the magnitude of the incident scattering force at $x = 0$ ($|\vec{F}_{00}^s| = 0.98 \pm 0.03 pN$) was given from the fit. This value is near calculations of scattering force magnitude on a Rayleigh particle using equation 1 in the work done by Ashkin et.al. [1] which yields $1.17 pN$. We assume the parameters of a 500nm diameter polystyrene particle ($n_p = 1.55$) trapped in water by a $1064nm$ laser ($\lambda = 800nm$ in water). The intensity of the incident beam at $x = y = 0$, I_0, can be calculated from the total power and the x and y widths of the 2D-Gaussian beam profile by $I_0 = P/(\sigma_x \sigma_y \pi) = 70mW/(15\mu m \cdot 0.5\mu m \cdot \pi) = 3.0mW/\mu m^2$.

the scattering and gradient force compensate each other. By examining the ray diagram in Fig. 4(a) it is expected that the gradient force distribution will be unchanged as the cylinder lens is shifted. The solid light rays (representing a non-zero angle of incidence of the trapping beam on the dichroic coverslip) are parallel to the dashed light rays (representing normal incidence of the trapping beam) before entering the objective lens, so when they emerge they must intersect in the focal plane. Thus it is expected that the intensity distribution in the trapping region near the reflective surface, which is situated near the front focal plane of the objective, must remain unchanged. Images of the intensity distribution on the surface of the dichroic coverslip were

#152071 - $15.00 USD Received 1 Aug 2011; revised 8 Sep 2011; accepted 8 Sep 2011; published 5 Oct 2011

obtained by removing the band pass filter (see Fig. 1) from the observation path to allow the laser light to be imaged on the CCD chip. Fig. 5(a) shows the intensity profiles along the *x*-axis as the cylinder lens is moved in steps of $50\mu m$. A shift of $\pm 4\mu m$ in the center position of the

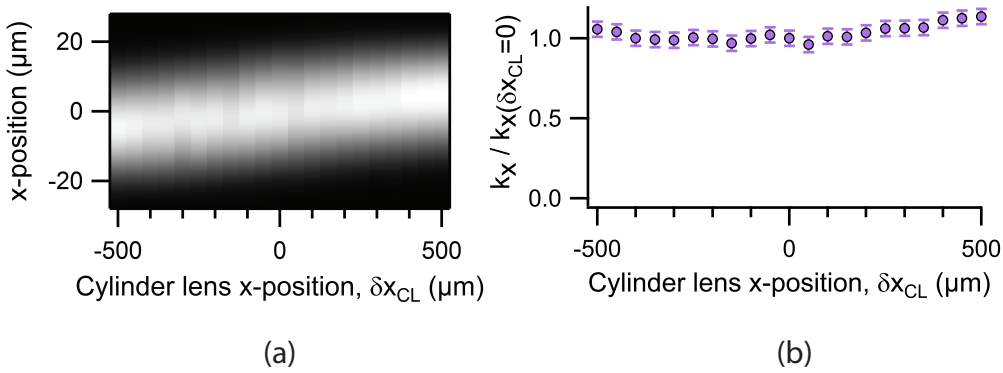

Fig. 5. Intensity profile of the SWOLT as a function of the position of the cylinder lens. a) The intensity profile of the trap is imaged directly to provide the gradient force component of the optical forces acting on the particles. No particles are in the trap. Each column of pixels represents the intensity profile of the trap along its length averaged over $\pm 250nm$ from the longitudinal axis ($y = 0$). Profiles were measured as the cylinder lens was translated in steps of $50\mu m$. b) Normalized longitudinal stiffness ($k_x/k_{x(\delta x_{CL}=0)}$) of the SWOLT as function of the cylinder lens position. The stiffness was calculated from the intensity distribution (see text).

intensity profiles can be seen as the cylinder lens is moved. This shift is a result of translating the cylinder lens without also translating the path of the incident laser beam. However, this shift is in the opposite direction of the particle displacement and is smaller in magnitude. Therefore the scattering force is pushing the particle to different locations in the trap rather than being moved to a new intensity maximum by the gradient force. To obtain a measure of the strength of the spring constant k_x, we analyzed the intensity profiles. By taking the derivative of each intensity profile, which is proportional to the gradient force, a line can be fitted to the derivative near the trap's center. The slope of this line is proportional to the spring constant. Figure 5(b) shows that the calculated magnitude of the spring constant remains unchanged as the cylinder lens position is varied. Thus the strength of the lateral scattering and the gradient force are independent within the tested range.

To describe the new equilibrium position of the trapped particle when the angle of incidence (θ_m) is not zero, we now develop a quantitative description of the lateral scattering force as a function of θ_m. The net scattering force can be described by:

$$\vec{F}^s_{net} = -2|\vec{F}^s_0|\sin(\theta_m)\hat{x} \tag{1}$$

where θ_m is the incident angle of the beam with respect to the normal of the reflective coverslip (see Fig. 4 and Fig. 6). $\vec{F}^s_0$ is the scattering force applied to the particle by the incident light ray. Assuming the particle is near the dichroic coverslip which has a reflectivity close to 100%, we can approximate the magnitude of the scattering force applied by the reflected light ray $\vec{F}^s_{ref}$ to be equal to that of the incident light ray (see Fig. 4(a) inset). If the particle is not trapped in the first antinode of the SWOLT (closest to the coverslip), but is trapped in an antinode further from the surface, this approximation will become less accurate for large incident angles θ_m since the incident and reflected rays striking the particles will have different intensities based

#152071 - $15.00 USD Received 1 Aug 2011; revised 8 Sep 2011; accepted 8 Sep 2011; published 5 Oct 2011

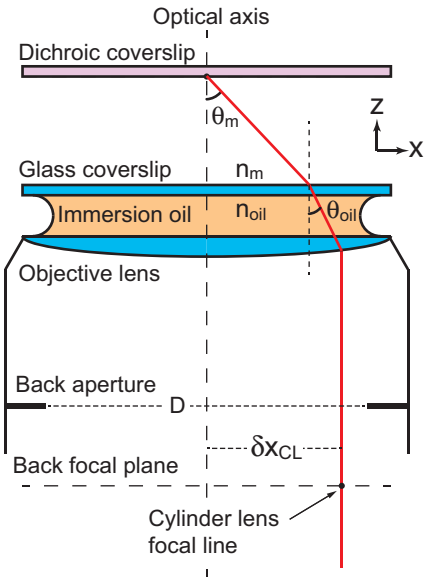

Fig. 6. Definition of the parameters used to calculate the incident angle of the laser light θ_m as a function of cylinder lens position δx_{CL}

on the intensity profile of the trapping beam. The magnitude of the force $\vec{F}_0^s$ is proportional to the intensity of the light ray generating that force. Since we can assume that the intensity profile of the beam is a Gaussian and the incident angle is independent of x-position in the SWOLT, we can write $\vec{F}_0^s(x) = \vec{F}_{00}^s \exp(-x^2/\sigma_x^2)$ where σ_x is the width of the Gaussian intensity profile in $\hat{x}$ and $\vec{F}_{00}^s$ is the incident scattering force at $x = 0$. Thus Eq. (1) becomes:

$$\vec{F}_{net}^s = -2|\vec{F}_{00}^s|\sin(\theta_m)e^{\frac{-x^2}{\sigma_x^2}}\hat{x} \tag{2}$$

To derive the relationship between the angle of incidence and the cylinder lens position, we use a simplified model of the objective lens as described by Hwang and Lee [50]. We consider a ray parallel to the optical axis whose distance from the optical axis corresponds to the center position δx_{CL} of the cylinder lens. The angle θ_{oil} can be related to the ray position δx_{CL} by:

$$n_{oil}\sin\theta_{oil} = \frac{\delta x_{CL}}{f} \tag{3}$$

where f is the focal length of the objective lens and n_{oil} is the refractive index of the immersion oil which is matched to that of glass. And in the limit where $\delta x_{CL} = D/2$ the equation becomes:

$$n_{oil}\sin\alpha_{oil} = \frac{D}{2f} \tag{4}$$

where α_{oil} is the maximum incident angle and is related to the numerical aperture NA of the objective lens by:

$$n_{oil}\sin\alpha_{oil} = NA \tag{5}$$

Using Snell's law, $n_m\sin\theta_m = n_{oil}\sin\theta_{oil}$, with Eqs. (3-5), we can write the incident angle θ_m as a function of the cylinder lens position δx_{CL}:

$$\sin\theta_m = \frac{2}{D}\frac{NA}{n_m}\delta x_{CL} \tag{6}$$

#152071 - $15.00 USD Received 1 Aug 2011; revised 8 Sep 2011; accepted 8 Sep 2011; published 5 Oct 2011

Thus the form of the scattering force and the gradient force acting on a particle along the x-axis in the SWOLT can be written as:

$$\vec{F}^{s}_{net}(x,\delta x_{CL}) = \frac{-4\,|\vec{F}^{s}_{00}|\;NA\;\delta x_{CL}}{D\;n_m}\; e^{\frac{-x^2}{\sigma_x^2}}\,\hat{x} \tag{7}$$

$$\vec{F}^{g}_{x}(x) = -k_x\,x\,e^{\frac{-x^2}{\sigma_x^2}}\,\hat{x} \tag{8}$$

where the x-component of the gradient force $\vec{F}^{g}_{x}$ is given by the gradient of a Gaussian intensity profile and is independent of cylinder lens position δx_{CL}. Using Eq. (7) and Eq. (8) it is now possible to solve for the equilibrium position of the particle, which is where $\vec{F}^{s}_{net} + \vec{F}^{g}_{x} = 0$. Solving these equations for x, the position of the particle, yields:

$$\vec{x}_{eqi}(\delta x_{CL}) = \frac{-4\,|\vec{F}^{s}_{00}|\;NA\;\delta x_{CL}}{k_x\;D\;n_m}\;\hat{x} \tag{9}$$

The validity of Eq. (9) can be tested by fitting this function against the experimental data (see Fig. 4(b)) leaving the magnitude of the maximal scattering force ($|\vec{F}^{s}_{00}|$) as the only free parameter. The excellent agreement of data and calculation confirms that our simple model is sufficiently precise to describe the change of the scattering and gradient force as a function of the position of the cylinder lens correctly.

If the gradient force does not change as the angle of incidence is changed, then a probe particle can be manipulated by the scattering force alone to an arbitrary equilibrium position along the trap. This allows us to measure the transverse stiffness of the trap k_y from the local thermal fluctuations of the particle (see Fig. 7). As expected, the transverse force constant,

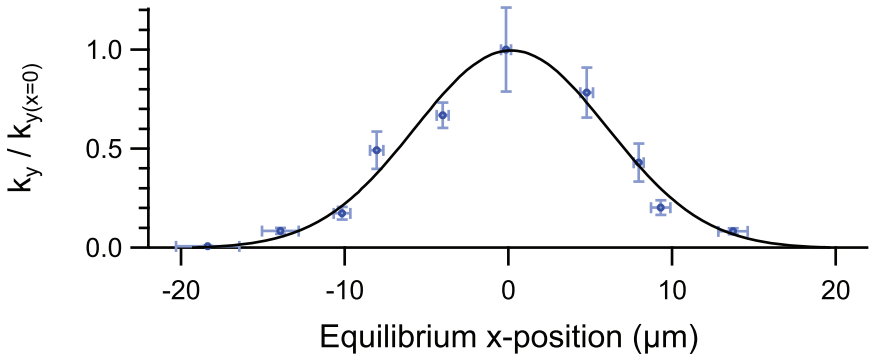

Fig. 7. Transverse stiffness of the SWOLT measured at different equilibrium positions along the trap. Using the lateral scattering force as shown in Fig. 4(a), a 500nm diameter polystyrene particle was pushed to positions away from the position of highest intensity. The transverse stiffness k_y was measured concurrently with equilibrium position data shown in Fig. 4(b). A Gaussian profile is drawn to guide the eye.

dominated by the gradient force, follows essentially the Gaussian intensity profile of the trap. When the particle is displaced $15\mu m$ from the center to either side, its transverse stiffness drops to just a few percent of its center value, but the trap is still strong. We like to emphasize again that the positioning of the particle was achieved by the lateral scattering force, in contrast to most other optical manipulation techniques in which the particle is transported primarily by the gradient force and thus typically comes to rest at the intensity maximum.

To quantify the lateral scattering force along the long axis of the trap, we track the probe particle as it is transported along the length of the trap to its rest position which is given by the

#152071 - $15.00 USD Received 1 Aug 2011; revised 8 Sep 2011; accepted 8 Sep 2011; published 5 Oct 2011

balance of the gradient and scattering force as calculated above. Since the Reynolds number of a nanoparticle in water is very small, it can be assumed that the particle/fluid system is overdamped and the particles travel at terminal velocity at any instant. In this case the drag and the optical force are always in balance, and we can determine the magnitude of the optical forces along the SWOLT from the local velocity of the particle using Stokes' law: $\vec{F}_x^d = 6\pi\varepsilon\eta a v_x \hat{x} = \vec{F}_{net}^s + \vec{F}_x^g$ where η is the viscosity of the fluid, ε is a correction factor for the viscous drag near a surface [51], a is the radius of the particle, and v_x is the x-component of the particle's velocity. Figure 8(b) shows the local velocities of particles and the corresponding forces while they are transported form the capture position to the position of zero force. The results are an average over 16 to 18 particles for each of the three angles of incidence. For the case of vertical incidence ($\theta_m \approx 0$) for which the scattering force is almost completely compensated, the force profile resembles that of the gradient of a Gaussian intensity profile as expected. When the incidence angle is not zero, a net scattering force ($\vec{F}_{net}^s$) is generated. With increasing angle of incidence, the maximum velocity of the captured particle increases, and the equilibrium position of the particle is moved further away from the center of the trap as already indicated in Fig. 4(b). We can calculate the local velocity of the particle as a function of the angle of incidence from Eqs. (2), (8), and Stokes' law:

$$\vec{v}_x(x,\theta_m) = \frac{-1}{6\pi\varepsilon\eta a} e^{\frac{-x^2}{\sigma_x^2}} \left[2|\vec{F}_{00}^s|\sin(\theta_m) + k_x x\right]\hat{x} \tag{10}$$

The data sets in Fig. 8(b) were fitted with Eq. (10) where the angle of incidence was the only free parameter. The resulting angles of incidence agree well with the experimental values calculated from the cylinder lens positions $\delta x_{CL} = \{0, -100, -200\} \pm 15\mu m$ (corresponding to $\theta_m = \{0, -2.62, -5.24\} \pm 0.39^\circ$). The uncertainty in cylinder lens position arises from the mechanical accuracy and drifting of the positioning stage. The good agreement between the model and data again supports the assumption that the scattering force can be varied independently of the gradient force.

So far, net scattering forces were generated by changing the angle of incidence of the collimated beam by displacing the cylinder lens perpendicular to the optical axis. However, scattering forces that lead to transport in the SWOLT can be generated in another way. Fig. 9 illustrates how lateral scattering forces can be generated by translating the cylinder lens along the optical axis rather than perpendicular to it. The forces now act radially inwards (converging beam) or outwards (diverging beam) from the optical axis, and the incident angle varies with the position along the long axis of the trap. For a diverging beam (Fig. 9(a)), the x-components of the scattering force counteract the gradient force and push the particles away from the center of the trap. For a converging beam (Fig. 9(b)), the net scattering force reinforces the gradient force and pushes the particles toward the center of the trap. The latter essentially leads to stronger confinement and a higher force constant of the trap. Also in this case, the intensity profile of the SWOLT near the surface of the dichroic coverslip will remain constant as the cylinder lens is translated along the optical axis (δz_{CL}). Thus the gradient force again remains constant even as the scattering force is varied. Using this technique, particles can be transported radially toward or away from the center of the SWOLT, rather than unidirectionally as shown earlier. Fig. 10 shows images of particles being positioned by translating the cylinder lens along the optical axis.

When the cylinder lens is moved towards the objective lens and a diverging beam is generated, the net scattering force acts radially outward and pushes the particles outward from the center of the trap, thus separating them as shown in Fig. 10(a). When the cylinder lens is moved away from the objective lens and a converging beam is generated, the particles are pressed together as shown in Fig. 10(c). We note that the inter-particle spacings seen in Fig.

#152071 - $15.00 USD Received 1 Aug 2011; revised 8 Sep 2011; accepted 8 Sep 2011; published 5 Oct 2011

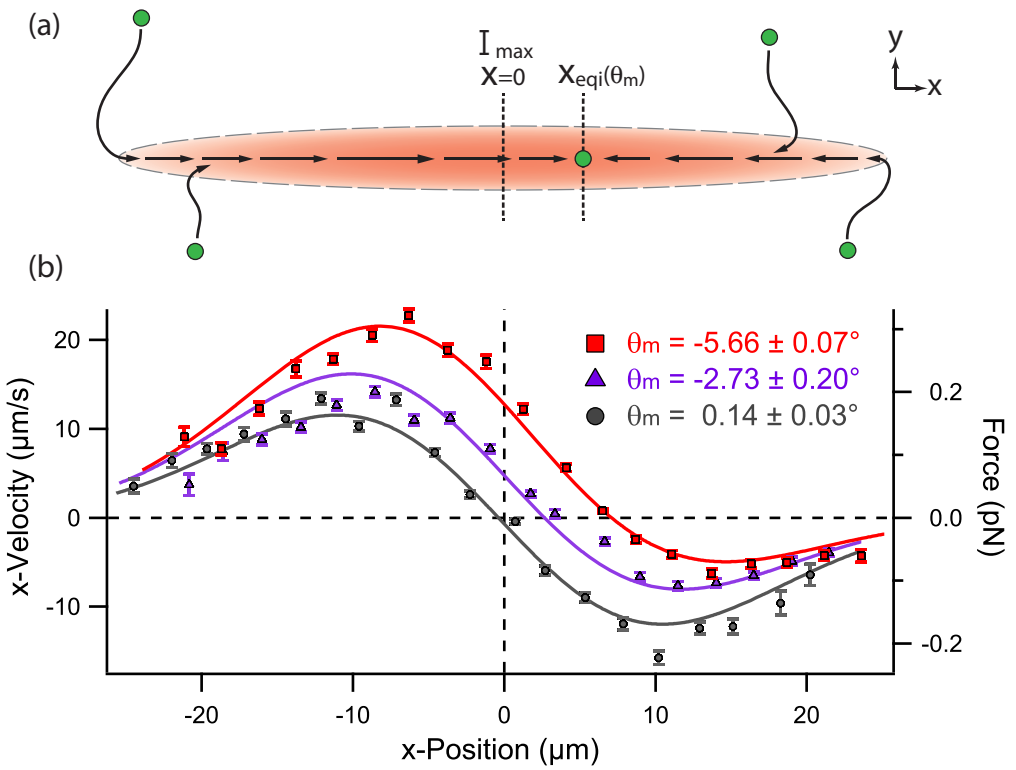

Fig. 8. Measurement of the optical force component along the long axis of the SWOLT: $\vec{F}_x^{Total}(x) = \vec{F}_{net}^{s}(x) + \vec{F}_x^{g}(x)$. To measure the forces acting along the entire length of the trap, particle velocities were measured. a) Experimental procedure. Particles diffuse one-by-one into the trap near one of the ends. A video is recorded of the particle being transported to its rest position which depends on the incident angle of the trapping beam θ_m. The positions and velocities of the particles are determined by video particle tracking. b) The average velocity of the particle at each position in the trap is shown for different angles of incidence (θ_m). The right axis shows the corresponding optical forces. The solid curves are fits from the model (Eq. (10)) where θ_m is the only free parameter. The remaining parameters are fixed to known, measured, or estimated values. $|\vec{F}_{00}^{s}| = 1pN$, $k_x = 25fN/\mu m$, and $D = 4277\mu m$ as described in Fig. 4. The particle radius ($a = 250nm$) is given by the manufacturer; the width of the Gaussian intensity profile ($\sigma_x = 15.5\mu m$) is measured from images of the intensity profile at the coverslip surface; the viscosity of water ($\eta = 1.0fNs/\mu m^2$) is known; and the viscous drag correction factor ($\varepsilon = 3$) was estimated for a particle moving near a surface [51]. Though the particles used here are large and are trapped near the surface, they do not make contact due to repulsive electrostatic forces. This occurs because both the glass surface and the carboxylated polystyrene particles naturally have a negative charge, and the Debye length in deionized water is very long compared to the glass-particle separation distance. Videos were recorded at a rate of 80 fps. The results of at least 16 particles were averaged for each measurement. The error bars represent the standard error of the mean of these measurements. All measurements were done using 70mW of laser power in the sample plane.

10 are determined in part by optical binding forces [52–56]. The SWOLT may provide a very efficient method for studying such optical binding forces.

Since both the methods, single-direction transport as in Fig. 4(a) and radial transport as in

#152071 - $15.00 USD Received 1 Aug 2011; revised 8 Sep 2011; accepted 8 Sep 2011; published 5 Oct 2011

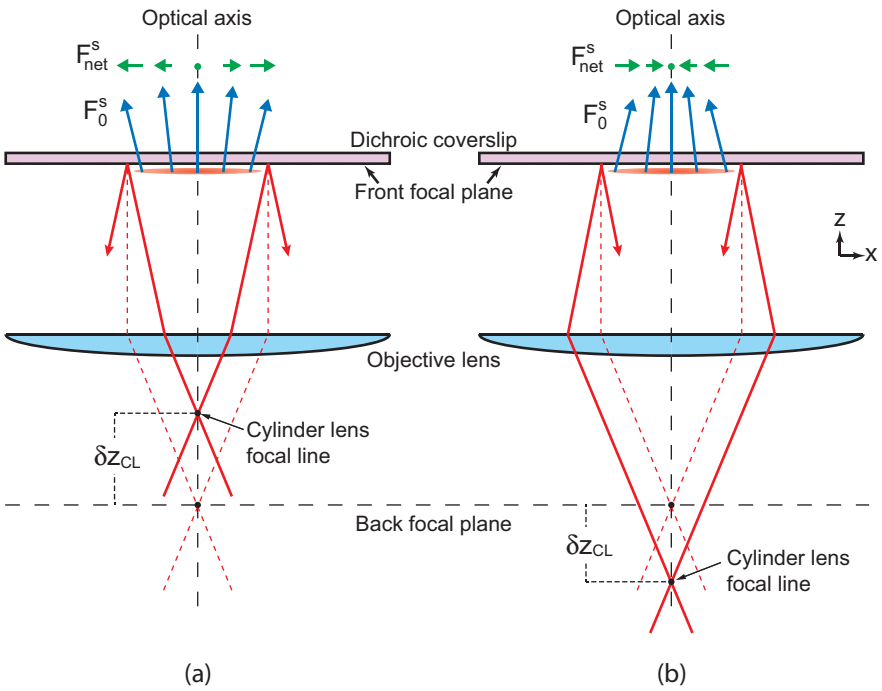

Fig. 9. Generation of axially symmetric scattering forces by translating the cylinder lens along the optical axis. a) Generation of radially outward pointing scattering forces by a diverging beam. b) Generation of radially inward pointing scattering forces by a converging beam.

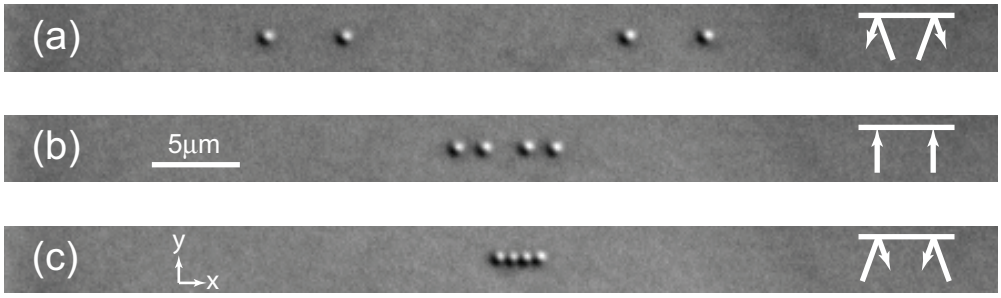

Fig. 10. Positioning of particles with radially symmetric scattering forces. a) Particles are pushed away from the center of the trap by the lateral scattering forces generated by a diverging beam ($\delta z_{CL} = 60mm$). b) Particles move closer to the center of SWOLT when the laser light is focused on the back focal plane of the objective lens ($\delta z_{CL} = 0$) and the net scattering force is reduced to 0. c) When the cylinder lens is moved away from the objective lens ($\delta z_{CL} = -140mm$) thus generating a converging beam, the particles are pressed closer together. Inset: Propagation of the light rays at the dichroic coverslip surface.

Fig. 9, allow for varying the net scattering force independently of the gradient force, they can be used to generate continuous transport of particles. Fig. 11(a) (Media 1) shows the continuous transport of particles in a single direction by increasing the angle of incidence of a collimated beam while Fig. 11(b) (Media 2) shows the continuous transport of particles in opposite directions by a divergent beam. Particles 500*nm* in diameter, carried by a flow of water, are captured

#152071 - $15.00 USD Received 1 Aug 2011; revised 8 Sep 2011; accepted 8 Sep 2011; published 5 Oct 2011

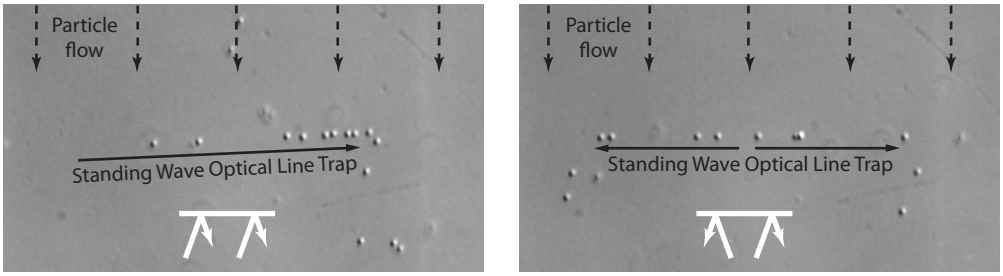

(a) (b)

Fig. 11. Single frame excerpts from video recordings of continuous transport in a SWOLT. Polystyrene particles are continuously transported by fluid flow into the SWOLT which lies perpendicular to the flow. The particles are then captured by the SWOLT and transported by the lateral scattering force towards the end(s) of the trap where the optical gradient force is much weaker. There, the drag force from the fluid flow is strong enough to overcome the gradient force and push the particle out of the trap. a) Single direction transport as illustrated in Fig. 4(b) with $\delta x_{CL} = -500\mu m$. The SWOLT is tilted slightly towards the fluid flow to show that the particle transport is not due to drag forces (Media 1). b) Bidirectional outward transport as illustrated in Fig. 9(a) with $\delta z_{CL} = 100mm$ (Media 2). The figure and media dimensions are $58\mu m$ by $32\mu m$.

by the SWOLT which lies perpendicular to the fluid flow. Since the cylinder lens has been translated perpendicular to or along the optical axis, a net scattering force is generated which pushes the particles toward the end(s) of the trap. Since the transverse spring constant k_y of the trap decreases significantly toward the ends of the trap (see Fig. 7), the drag force on the particles is sufficient to overcome the optical gradient force there and carry the particles out of the trap. Thus continuous transport is generated in the SWOLT by combination of the strong gradient force that captures the particles from the flow and the strong lateral scattering force that pushes the particles over long distance to unstable regions where they leave the SWOLT.

4. Conclusion

We demonstrated that stable confinement and precise alignment of nanoparticles can be achieved in a standing wave optical line trap at low laser power. 100nm gold particles were stably trapped in the SWOLT with power densities more than 3 times smaller than needed in a single beam trap. The increase in stability is due to the compensation of the axial scattering force which lowers the stability of conventional single beam gradient traps. While the axial scattering force is compensated, there is an amplification of lateral components that can be used to manipulate the position of particles within the SWOLT. The gradient force that causes the transverse confinement remains essentially unaffected by the manipulation of the scattering force, i.e. particles can be manipulated without altering the confinement properties of the trap. In this way, particles can be transported with varying velocities along a well-defined path and over long distances ($> 40\mu m$). In principle, the length of the SWOLT is only limited by the aperture of the front lens of the objective. In our case, this would be about $1.35mm$ (given by the manufacturer). Thus, provided there is enough laser power, transport should be possible over much longer distances than shown here. Continuous transport can be achieved by utilizing the lateral scattering force to push particles into positions of weak confinement. There, they can be more easily retrieved from the trap and collected, thus creating space for new particles to enter the trap and be transported. In this work, for example, a fluid flow was used to both intro-

#152071 - $15.00 USD Received 1 Aug 2011; revised 8 Sep 2011; accepted 8 Sep 2011; published 5 Oct 2011

duce particles into the trap and retrieve them from the end of the trap. It might be possible to use multiple SWOLTs to hand off particles from one SWOLT to another which would allow for continuous sorting or mixing of particles. In an advanced arrangement, a three step process can be employed where nanoparticles are first sorted, then arranged, and finally brought together and assembled. The standing wave optical line trap provides the precision necessary to achieve this kind of controlled assembly of nanoparticles in solution at room temperature.

Acknowledgments

The authors would like to thank Kathleen Hinko and Pinyu Thrasher for helpful discussions and Alexandr Jonáš for careful reading of the manuscript and helpful comments.

#152071 - $15.00 USD Received 1 Aug 2011; revised 8 Sep 2011; accepted 8 Sep 2011; published 5 Oct 2011